Cement & Concrete Composites 45 (2014) 234–242

Contents lists available at ScienceDirect

Cement & Concrete Composites

journal homepage: www.elsevier.com/locate/cemconcomp

High temperature resistance of a very high volume fly ash cement paste

Shane Donatello [a,*], Carsten Kuenzel [b], Angel Palomo [a], Ana Fernández-Jiménez [a]

[a] Eduardo Torroja Institute of Construction Sciences (CSIC), C/Serrano Galvache 4, 28033 Madrid, Spain
[b] Imperial College London, Exhibition Road, South Kensington, London SW7 2AZ, UK

ARTICLE INFO

Article history:
Received 18 February 2013
Received in revised form 11 August 2013
Accepted 14 September 2013
Available online 21 September 2013

Keywords:
High temperature resistance
Durability
Sintering
Fly ash
Hybrid alkaline cement
Paste

ABSTRACT

The physical and chemical changes taking place in a very high volume fly ash cement paste (FAN-4) following exposure to temperatures up to 1000 °C are presented. Tests were repeated with commercially available CEM II/A-M Portland composite-cement (MS). FAN-4 pastes showed impressive residual strengths after heat exposure which increased dramatically when heated previously at 800 or 1000 °C. This was in stark contrast to the MS paste, which showed a continual decrease in residual strength following heating and subsequent cooling. The increase in residual strength with FAN-4 paste coincided with a major shrinkage event, which was associated with sintering and the formation of the new mineral phases anorthite, gehlenite, wollastonite, diopside and albite. The MS cement formed generally non-hydraulic calcium silicate phases upon heating at $\geqslant$800 °C. The differences in phase formation were linked to different starting elemental compositions. The FAN-4 paste was considerably richer in Si, Al, Fe and alkalis but poorer in Ca. The elemental composition of the binder phase will be an important factor to take into account when determining the high-temperature performance of future cements and concretes, which are likely to contain significantly higher contents of supplementary cementitious materials than is presently the case.

1. Introduction

1.1. Lowering the CO_2 footprint of Portland cement based materials

While significant improvements in the Portland cement (PC) manufacturing process have been made by shifting from the wet process to the dry process and introducing pre-heating and pre-calcining stages [1,2], it is unlikely that further major improvements in thermal efficiency of the process can be made [3]. It is widely regarded that the key to further major reductions in the CO_2 emissions associated with PC manufacture is to increase the quantity of blended materials in cements, i.e. to reduce the mass of clinker in a given mass of cement by blending with industrial by-products, natural pozzolans or calcined clays [2,4–5].

Arguably the most significant industrial by-product with regards to blended cements is coal fly ash. Rough estimates for global fly ash production in 2010 are around 800–1000 Mt although the exact figure is difficult to ascertain since in many countries coal power stations are not obliged to report this data. From a life cycle assessment perspective, it is feasible to consider available fly ash as a CO_2 free resource. Fly ash has been used in blended cements for decades at replacement rates of around 10–30% as is reflected by various national and international standards [6–7]. More recently work has been carried out investigating the use of blended cements with significantly higher fly ash contents [8–10]. One major issue with high fly ash content cements is slow setting and low early strengths. One possible approach to minimising this problem, while maintaining high cement replacement rates, has been to create ternary blended cements with fly ash, limestone and PC [11,12]. Another approach has been to add a source of strong alkali to activate fly ash glassy phases much more rapidly than is the case with the typical pozzolanic reaction with portlandite at ambient temperature [13,14]. With regards to the latter approach, the blended cements can be termed as "hybrid alkaline cements".

While drastically reducing the CO_2 emissions associated with the binder, the effect of the high fly ash content on durability aspects of pastes is uncertain. In a recent publication by the authors, the high fly ash content cement pastes and mortars were shown to present a similar resistance to Na_2SO_4, seawater and acid solutions as a commercially available sulphate resistant PC [15]. Another important durability aspect is resistance to high temperatures, which provides a useful indicator of the behaviour of a material during a fire event.

1.2. High temperature exposure of Portland cement and concretes

Cement based materials are non-flammable and offer significant safety advantages over wood and plastic and help protect

* Corresponding author.
E-mail address: shanedonatello@hotmail.com (S. Donatello).

0958-9465/$ - see front matter © 2013 Elsevier Ltd. All rights reserved.
http://dx.doi.org/10.1016/j.cemconcomp.2013.09.010

steel rebar in structural concretes. However, fire events and high temperature exposure can nonetheless cause significant damage to PC based materials.

In a normal PC paste, pore water and crystalline hydration water can be lost from AFt and AFm type phases and C–S–H gel at temperatures below 300 °C [16]. Despite this, it is worth mentioning that some pastes can exhibit strength increases following heating at 105 °C [17,18]. Such unusual behaviour is likely to be due to trapped steam vapour creating conditions favourable for the in situ hydrothermal synthesis of C–S–H type phases.

As the temperature increases, the dehydration of portlandite, another major product in PC pastes, generally occurs between 400 and 550 °C [19] and provokes a significant shrinkage effect [20]. The presence of dehydrated portlandite leaves the microstructure prone to expansion upon subsequent rehydration, which is an exothermic reaction, as indicated by the reverse reaction of Eq. (1) [19,21]. The rehydration of portlandite is well known to be detrimental to cement pastes and concretes and the degree of degradation can be directly linked to the sorptivity of heat exposed PC pastes and concretes [22]. Due to the restricted movement of water through the pore network of the solid matrix, water removed by C–S–H, AFt/AFm and portlandite dehydration can be retained within the matrix as steam vapour, with pressures building up to a point at which cracks are produced and surface spalling can occur as tiny pockets of high pressure vapour are explosively released. Considerable research effort has been focussed on trying to understand the key factors behind the spalling process [23,24]. The performance of cements and concretes containing pozzolanic additions has been shown to be beneficial in cases where blast furnace slag [25] or volcanic ash [26] were used. While this could simply be attributed to the lower portlandite content, such an explanation would fail to account for irregular results with silica fume blended cements [27,28].

$$Ca(OH)_2 \leftrightarrow CaO + H_2O \quad \Delta H = +65\ kJ/mol \quad \text{(forward reaction)} \tag{1}$$

$$CaCO_3 \leftrightarrow CaO + CO_2 \quad \Delta H = +178\ kJ/mol \quad \text{(forward reaction)} \tag{2}$$

Another aspect to consider is the decomposition of calcite to free lime, which generally occurs at temperatures of 600–850 °C (see Eq. (2)). The free lime produced by decarbonation, like that from portlandite dehydration, is liable to later hydrate into expansive $Ca(OH)_2$. At higher temperatures, sintering of silicate phases can occur and provoke major changes in sample density, dimension and crystalline components. The hybrid alkaline cement used in this study is likely to behave in a much different manner to a pure PC paste at sintering temperatures (typically 800–1100 °C) due to its high fly ash content. Another important consideration may be the significant quantity of quartz introduced with the fly ash component. Quartz is known to exhibit a sudden expansion at 573 °C following conversion from low α to high β type quartz [18,19].

The general effect of replacing cement clinker with a class F fly ash is to reduce the quantity of Ca in the paste and therefore the quantity of portlandite and calcite present. Any free $Ca(OH)_2$ will either carbonate or sooner or later be locked into C–S–H or C–A–S–H type gels via the pozzolanic reaction of portlandite with fly ash glassy phases [29]. According to Khoury [18], this should help improve resistance to degradation at high temperatures and was indeed reflected in a large number of tests carried out on cement pastes and concretes exposed to 600 °C [30]. However, many other aspects such as differences in the gel structure, Ca:Si ratios of gels, w/b ratios and the nature of any aggregates used may also be important.

As part of a larger set of trials, the objective of this work is to evaluate the resistance of a novel hybrid alkaline cement containing a very high content of fly ash (ca. 80% by mass) to high temperature environments in comparison with a PC based reference paste. Although many other factors such as aggregate type and specimen dimensions will undoubtedly be important, in order to focus solely on the behaviour due to the nature of the binder composition at high temperatures, tests were carried out with pastes, and then only with specimens of identical dimensions.

2. Materials and methods

2.1. Materials

The very high volume cement binder (FAN-4) consisted of a class F fly ash milled until ⩾98% of the sample passed a 45 μm sieve, a PC clinker milled until ⩾85% passed a 45 μm sieve and a laboratory grade Na_2SO_4 salt (Panreac). Further details of the hybrid blend composition and raw material compositions can be found in an earlier publication by the authors [14].

As a reference material, a commercially available Type II/A-M Portland-composite cement (MS) was also tested under the same conditions as used with the test hybrid cement (FAN-4). According to the EN 197-1 [7] definition of Type II/A-M cements, between 6% and 20% of cement by dry mass had been substituted by an unspecified pozzolanic material or blend of pozzolanic materials, such as coal fly ash, blast furnace slag or natural pozzolans. Furthermore, up to 5% content as limestone is also permitted. Due to obvious economic and environmental reasons, blended Portland cement is becoming more common on the market at the expense of pure (CEM I type) Portland cements. Type II/A-M cements are particularly attractive since they afford significant flexibility to the manufacturer in cement formulation and make it harder for competitors to copy any successful blends. In terms of total dry content as PC clinker, the hybrid FAN-4 paste contains only 18% clinker (Ca poor) whereas the reference Type II/A-M cement will contain around 80–90% clinker (Ca rich). The major elemental compositions, as determined by X-ray fluorescence (Philips PW 1404/00/01), of the two anhydrous cements are shown in Table 1.

2.2. Paste elaboration

Pastes were mixed together with distilled water using the minimum liquid to binder ratios possible while maintaining sufficient workability of the paste. The liquid to solid ratios were 0.36 and 0.32 for the FAN-4 and MS pastes respectively. Pastes were mixed manually for 3 min and cast into 1 × 1 × 6 cm stainless steel moulds with the aid of a jolting apparatus. Moulds were then placed in a curing chamber maintained at 23 ± 2 °C and ⩾95% relative humidity. After 24 h, samples were demoulded and left to continue curing in the humidity chamber for a period of 70 d before being subjected to the high temperature resistance tests.

2.3. High temperature resistance tests

Paste samples were weighed, measured and photographed prior to being exposed to either: 200, 400, 600, 800 or 1000 °C for a

Table 1
Major element composition determined by XRF (expressed as oxides in wt.%).

	SiO_2	Al_2O_3	CaO	Fe_2O_3	MgO	Na_2O	K_2O	SO_3	LOI[a]
FAN-4	48.7	17.1	13.5	7.4	1.8	1.8	2.1	2.2	4.4
MS	26.3	6.8	46.6	2.5	4.8	1.0	1.0	6.4	4.0

[a] LOI represents weight "loss on Ignition" at 1000 °C during 1 h in Pt crucibles.

period of 1 h. Exposure was achieved by direct placement in an oven pre-heated to the test temperature. Immediately after removing from the oven, half of each sample batch was left to cool on a ceramic plate in air ('slow' cooling) and the other half was cooled by immersion in tap water for 15 min (rapid cooling) then left to dry on paper towels in air. Although both methods can be considered as relatively fast cooling procedures, immersion in water is even faster than in air and is an important consideration due to the fact that in real life, most fires are extinguished with water and the subsequent rehydration of fire damaged cement based materials is a particular concern.

Samples were left overnight to dry on a laboratory bench and then reweighed, measured and photographed. The $1 \times 1 \times 6$ cm samples were then tested for flexural strength via a 3 point loading test with prisms centred upon two supports spaced 50 mm apart (NET-ZSCH 6.111.2 GmbH). The load was applied from above on the centre of the specimen and the flexural strength limit calculated according to Eq. (1) for samples with rectangular cross sections.

$$F = \frac{3.P.L}{2.b.d^2} \tag{3}$$

where is the F the flexural strength (MPa); P the maximum load at failure (N); L the distance between lower support spans (50 mm); b the average width of sample (10 mm); and d is the average height of sample (ca. 10 mm)

The flexural strength test produced a single fissure in the centre of the prism. The two fragments were each then tested for compressive strength across a 10×10 mm platen with a loading rate of 0.07 kN/s applied (Ibertest Autotest 200/10/SW). Strengths of pastes not subjected to high temperatures were also tested as a baseline control. After testing, some fragments of each sample batch were ground to a fine powder and analysed by X-ray diffraction (Bruker D8 Advance). Changes in microstructure and paste reaction products were analysed by Field Emission SEM with EDX analysis of broken paste fragment surfaces (Hitachi S-4800).

Normally hydrated paste prisms (70 d old) were also tested with a dilatometer (Netzch 402E). This technique measures the movement of alumina pushrods that are pressed on the axial ends of the prismatic test specimen with a force of 20cN. The sample chamber was also made of alumina. Any expansion or shrinkage of the prism is reflected by the movement of these pushrods and is recorded by a data logger as a function of test time and chamber temperature. Tests were carried out over the range 20–1000 °C at a heating rate of 10 °C min^{-1} in a He atmosphere. Finally, nonheat treated pastes were also analysed by simultaneous TG-DTA (thermo-gravimetric-differential themal analysis – TA SDT Q600 analyser) in an air atmosphere from 30 to 1000 °C at a heating rate of 10 °C/min.

3. Results

3.1. Visual changes in paste samples

Visual changes to pastes are illustrated in Fig. 1 for both FAN-4 and MS pastes.

From the images in Fig. 1 it is clear that different reactions are taking place in each paste system. In the FAN-4 paste, a progressive lightening of the original dark grey colour was apparent after heating at 400 and 600 °C. Heating up to 800 °C caused an abrupt change to an orangey-red colour which then evolved to a pale red colour upon heating at 1000 °C. This behaviour is characteristic of changes in Fe compounds present in fired FAN-4 pastes and is analogous to the process that is well known in the brick industry for producing the orange–red–pink hues in bricks [31,32]. Partial fissures were noted in 800 and 1000 °C heated pastes.

With the MS reference paste, very little change in the paste colour was noted even after exposure at 800 °C. However, after reaching 1000 °C, a distinct yellow colour was noted in both air and water-cooled pastes. This is likely to be due to the formation of Sulfur deposits from the decomposition of sulphides present in any blast furnace used in the MS cement. Fissures were noted in MS pastes from 400 °C and upwards, sometimes leading to complete fracture across the prism.

3.2. Changes in mechanical strengths of pastes after heat exposure

Changes in relative compressive strength and flexural strength as a function of cement type, cooling method and temperature are summarised in Fig. 2a and b.

The results in Fig. 2 reveal a number of differences between FAN-4 and MS paste mechanical strength responses to heat exposure, particularly in compressive strength behaviour. While MS pastes showed a gradual decrease in compressive strength up to 600 °C, losses in FAN-4 pastes were notably lower. However, the major change was at temperatures >600 °C, where FAN-4 paste residual compressive strengths increased by around 100% while MS pastes showed continued drops in residual strength. Compressive strength trends were generally similar for both air and water cooled pastes of a given cement.

With regards to flexural strength data, the cooling method had a much greater influence on results. MS pastes heated at $\geqslant$400 °C and air cooled became extremely brittle. None of the 400 °C MS samples were able to be tested (hence the discontinuation in the solid MS line in Fig. 2b). At higher temperatures, only 1 or 2 of the 4 MS replicates were able to be tested for flexural strength. Beyond exposure temperatures of 200 °C, residual flexural strengths in FAN-4 samples were consistently higher.

3.3. Length and weight changes in prismatic specimens after heat exposure

The MS pastes exhibited extremely stable dimensions over the entire temperature range when cooled in water but a steady shrinkage when cooled in air. These tendencies suggest that the expansion caused by the rehydration of free lime by cooling water was sufficient to compensate for thermal shrinkage caused by the initial dehydration reactions. In contrast, the cooling method had no significant influence on the shrinkage tendencies of FAN-4 pastes.

The degree of shrinkage in FAN-4 pastes was quite small and steady until 600 °C, after which a major shrinkage event was noted in FAN-4 pastes between 600 and 800 °C. This event coincided with the sudden increases in compressive strengths noted in Fig. 2 and such a combination is typically characteristic of a major sintering event. To study this event in more detail, dilatometric analysis of the pastes was carried out in order to better isolate the temperature at which this event occurred in the FAN-4 paste.

Dilatometry data for MS paste in Fig. 4 reveals a slight shrinkage between 200 and 500 °C, which can be attributed to dehydration of the specimen, followed by slight expansion between 500 and 800 °C, which may be attributable to simple thermal expansion of the specimen. Between 900 and 1000 °C, MS paste began to shrink significantly.

With FAN-4 pastes, marginal shrinkage between 150 and 350 °C can be attributed to dehydration. The major shrinkage event in FAN-4 pastes between 600 and 800 °C (as indicated by Fig. 3b) is confirmed and its onset pinpointed at around 705 °C. The degree of shrinkage measured in FAN-4 pastes with dilatometry apparatus was considerably larger (ca. 9%), than when prisms were manually

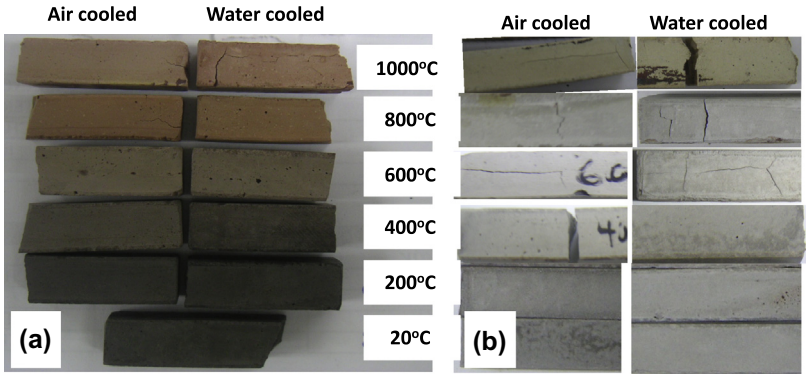

Fig. 1. Changes in visual aspect of (a) FAN-4 and (b) MS paste samples after exposure to different temperatures and cooling by water immersion or air convection.

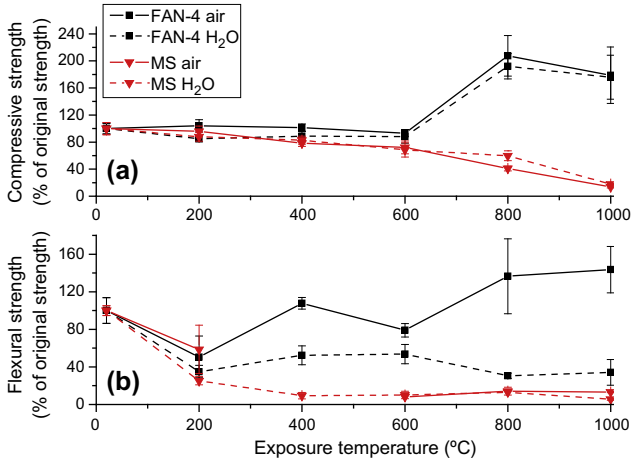

Fig. 2. Relative changes in (a) compressive strength and (b) flexural strength of MS and FAN-4 pastes as a function of cooling method (air or water) and exposure temperature. Note that results are the average of 4 measurements for flexural strength or 8 measurements for compressive strength. Original compressive strengths were 33.2 (100% for FAN-4 data) and 66.0 MPa (100% for MS data). Original flexural strengths were 7.2 MPa (100% for FAN-4 data) and 11.6 MPa (100% for MS data).

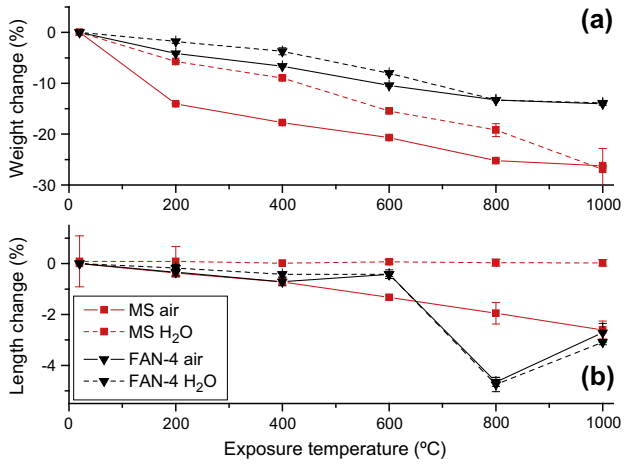

Fig. 3. Change in paste weight (a) and length (b) as a function of temperature exposure and cooling method.

measured with calipers after removing from the oven and cooling (ca. 5%, see Fig. 3). The most likely reason for this difference is that the former was measured in situ at high temperatures and the

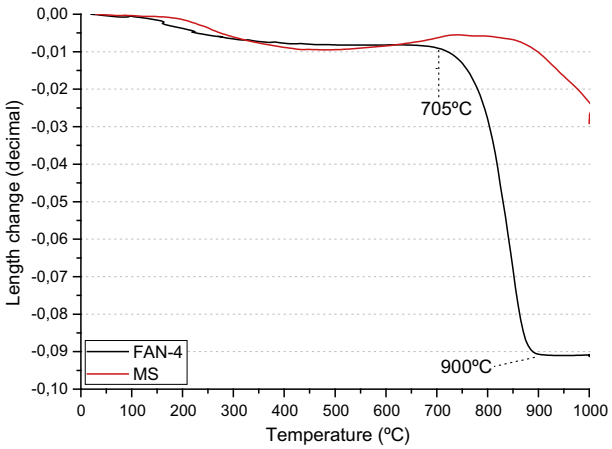

Fig. 4. Diatometric data of in situ measured MS and FAN-4 paste prism length changes during heating in a He atmosphere up to 1000 °C at 10 °C/min.

latter only after cooling overnight. The dilatometry data also reveal that the FAN-4 paste shrinkage halts at 900 °C, remaining stable up until 1000 °C at the end of the test.

The two general trends in weight changes shown in Fig. 3 are that weight loss was much greater in MS pastes than FAN-4 pastes and that for a given paste, losses were less in H_2O cooled samples than air cooled ones. This latter observation is only logical considering that cooling water can be reabsorbed and also reacts with free lime to form portlandite. Since MS cement contained much higher quantities of cement clinker phases, it is logical that MS pastes also contain higher quantities of C–S–H type gel, ettringite, portlandite and calcite and thus the greater general weight losses observed up to 800 °C.

Weight losses in FAN-4 pastes were much lower in general. Lower losses up to 200 °C imply that the combined quantity of crystalline water in gel and AFt/AFm type products was much lower than in MS pastes. Again this is only logical given the much lower contents of clinker phases present in FAN-4 pastes. Unlike the MS pastes, no sudden change in weight loss was noted between 800 and 1000 °C when cooled in water. This implies that unlike with MS pastes, no significant quantities of water soluble compounds were formed in FAN-4 pastes at 1000 °C.

Weight losses in the two pastes were also examined by simultaneous TG-DTA from 30 to 1000 °C in an air atmosphere at a heating rate of 10 °C/min. The results shown in Fig. 5 reveal that weight losses from fine powdered paste samples (both previously air dried) generally corresponded well to weight losses of complete prismatic paste specimens. The simultaneous differential thermal

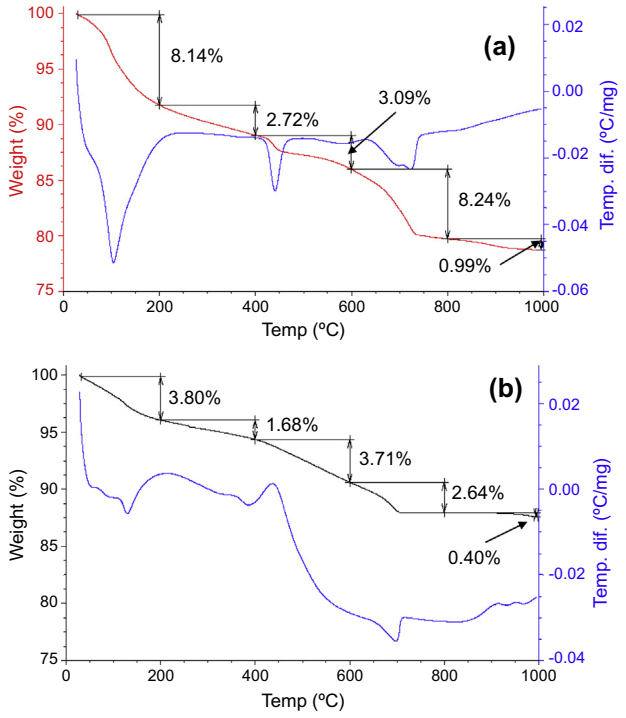

Fig. 5. Simultaneous TG-DTA data for (a) air cooled MS paste and (b) air cooled FAN-4 paste. Note that samples were heated from 30–1000 °C at a rate of 10 °C/min in an air atmosphere.

analyses also included in Fig. 5 reveal that a significantly higher quantity of absorbed/crystalline water from gels and AFm/AFt was lost from MS pastes (ca. 8%) than from FAN-4 pastes (ca. 4%) during heating up to 200 °C. In the 200–600 °C range, the main thermodynamic event in the control MS paste was clearly the dehydroxylation of portlandite. However, the FAN-4 paste showed a completely different thermal profile in this section. Instead of a clear endothermic peak due to portlandite dehydroxylation, two small exothermic peaks at around 350 and 430 °C were noted. Given that a general weight loss was observed in this region, it is likely to be due to combustion of traces of residual organic matter present. Another reason for differences in this temperature region is likely to be the higher Iron content of the FAN-4 paste. The oxidation of Fe or FeOOH to Fe_2O_3 and crystalline changes in Fe_2O_3 cystalline structures have been considered to occur in pure fly ash cements at these temperatures [33]. Finally, both samples show distinct decarbonation events at around 700 °C.

3.4. Changes in crystalline phase composition of pastes after heat exposure

From the strength and shrinkage results presented, examination of FAN-4 paste chemistry and microstructure at temperature exposures above and below 700 °C, is of considerable interest. Fig. 6 below compares nonheat-treated FAN-4 paste XRD data with that of pastes exposed to 400 °C and 800 °C after air cooling.

Prior to high temperature exposure, the FAN-4 paste was completely free of portlandite but contained a significant degree of calcite and a small amount of gypsum. The main fly ash phases were also noticeable; quartz (Q), anorthite (a), maghemite (M) and hematite (h). The glassy amorphous halo typical of fly ashes was noted via a background hump between approximately 18 and 35° 2Θ. Some unhydrated belite (B) was also evident. The key component of the paste, the cementitious gel, is XRD amorphous and can give rise to a background halo in diffraction spectra.

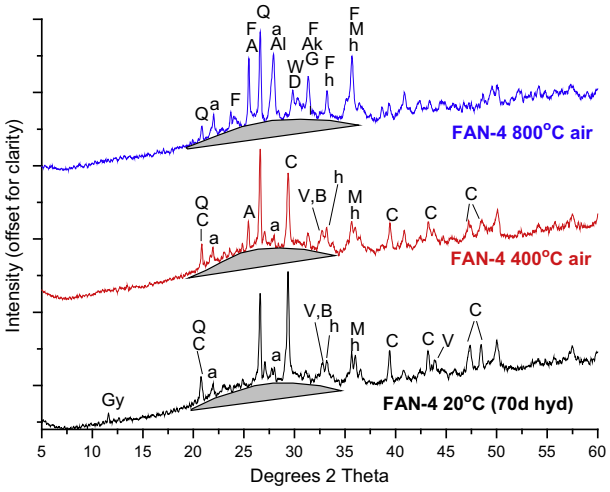

Fig. 6. XRD data of selected FAN-4 pastes. Peak labels are A – anhydrite ($CaSO_4$), a – anorthite ($CaAl_2Si_2O_8$), Ak – akermanite ($Ca_2Mg(Si_2O_7)$), Al – albite ($NaAlSi_3O_8$), B – belite (Ca_2SiO_4), C – calcite ($CaCO_3$), D – diopside ($CaMgSi_2O_6$), F – iron silicates (Fayalite Fe_2SiO_4 and Laihunite $Fe_{1.6}SiO_4$), G – gehlenite ($Ca_2Al(AlSiO_7)$), Gy – gyspum ($CaSO_4.2H_2O$), h – hematite (Fe_2O_3), M maghemite (Fe_2O_3), Q – quartz (SiO_2), V – vaterite ($CaCO_3$) and W – wollastonite ($CaSiO_3$).

However, it was not possible to distinguish any gel halo from the halo due to glassy phases originally present in the fly ash.

The presence of gypsum in non-fired pastes is supported by the appearance of the anhydrite at 25° 2Θ in 400 and 800 °C treated pastes. After heating to 800 °C, major strength gains and shrinkage were observed in FAN-4 pastes. This was associated with clear changes in crystalline phases present although the background amorphous hump did not change significantly. All peaks due to calcite or vaterite disappeared and new crystalline phases, potentially corresponding to albite (Al), wollastonite (W) gehlenite (G) and possibly anorthite (a) and diopside (D) were noted. Another new crystalline phase noted at 800 °C, which may have a significant role in the sintering process for FAN-4 pastes, was Laihunite (F) a Fe-silicate.

For comparison, XRD data for MS pastes before and after heat treatment are also included in Fig. 7.

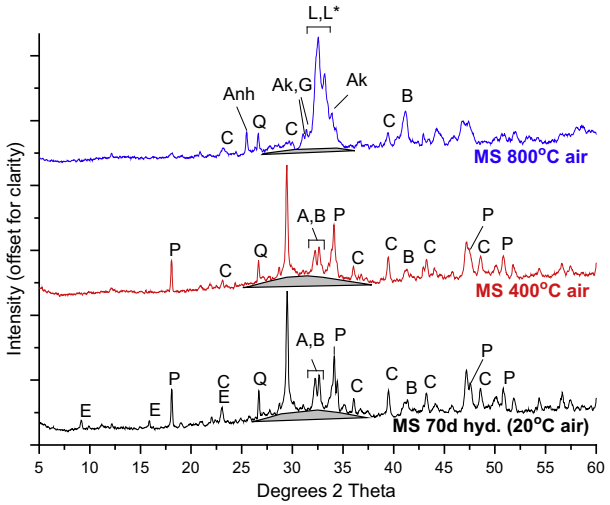

Fig. 7. XRD data of MS pastes before and after selected heat treatments. Peak labels are: A – alite ($3CaO.SiO_2$), Ak – akermanite ($Ca_2Mg(Si_2O_7)$), Anh – anhydrite ($CaSO_4$), B – belite (Ca_2SiO_4), C, calcite ($CaCO_3$), E – ettringite ($3CaO.Al_2O_3.3CaSO_4.26H_2O$), G – gehlenite ($Ca_2Al(AlSiO_7)$), L – larnite ($Ca_2SiO_4$), L* – (various Ca and Ca/Mg silicates), P – portlandite ($Ca(OH)_2$), Q –quartz (SiO_2).

The hydrated MS paste is typical of any PC paste. The diffraction pattern of the non-heated paste is dominated by the main calcite peak at 29° 2Θ. The broad and diffuse diffraction at the base of this peak is characteristic of amorphous C–S–H gel [34]. In general, a broad background halo, most likely due to the unspecified minor content of slag, was noted between 26 and 34°. Other important peaks are due to portlandite, ettringite and some unhydrated alite/belite. The presence of a quartz peak at 27° is a result of MS cement having been blended with minor quantities of unspecified pozzolanic additions. After treatment at 400 °C, the only notable change in crystalline phases was the disappearance of ettringite signals. However, after treatment at 800 °C, portlandite peaks disappeared, calcite peaks were greatly reduced and the formation of a dominant broad set of peaks due to poorly ordered crystals diffracting between 32 and 34° 2Θ appeared. Diffraction in this particular region corresponds well to alite and belite as well as non-hydraulic phases such as akermanite, gehlenite and numerous polymorphs of Ca disilicate and other Ca/Mg silicates (denoted L* in Fig. 6). An interesting point is that the amorphous C–S–H gel halo from 26–34° 2Θ disappeared after heating at 800 °C, while the new broad diffraction peaks appeared. This implies a structural reorganisation of the gel phase and minor slag component to form poorly ordered Ca–silicate and Ca/Mg silicate crystalline phases after heating at 800 °C.

3.5. Changes in FAN-4 paste microstructure after heat exposure >700°C

To visually confirm that the changes observed in FAN-4 pastes between 600 and 800 °C were due to sintering, the pastes heated at 600 and 800 °C were analysed by SEM–EDX. The key results are summarised in Fig. 8.

The images in Fig. 8 reveal an abrupt change in sample microstructure between 600 and 800 °C exposure. At 600 °C the morphology of the paste broadly resembles that of a normal cement gel fracture surface, with irregular and amorphous nodules and agglomerates. Fly ash cenospheres were clearly visible throughout the paste and the Si:Al ratio was generally 2:1 with variable contents of Ca depending on the proximity of the EDX point to underlying non-reacted fly ash particles. Contrary to XRD evidence, no examples of stand-alone anhydrite crystals were found. Point 4 in the EDX data of Fig. 8 was the most concentrated level of S found in the microstructure.

When the paste was treated at 800 °C, evidence of the formation of a molten vitreous phase was clear throughout the sample via the presence of continuous smooth structures with holes where gaseous products have bubbled off. The EDX points in image 8b show a significant enrichment of Ca at the general expense of Al in the molten phase. In XRD data, the main peaks for Ca–Mg silicate phases such as diopside ($CaMgSi_2O_6$) and akermanite ($Ca_2Mg(Si_2O_7)$) coincided with those for other likely products free of Mg such as wollastonite ($CaSiO_3$) and gehlenite ($Ca_2Al(AlSiO_7)$). Although SEM–EDX data implies that Mg is actively involved in the molten phase, due to the limited quantities of Mg available, the XRD peaks are likely to be dominated by the non-Mg containing phases.

4. Discussion

The results have revealed that unlike reference PC paste, FAN-4 pastes retain their compressive strengths when cooled after exposure to high temperatures up to 700 °C. At around this temperature, the pastes undergo a sintering process that causes significant shrinkage (5–9% depending on how it is measured) and a major increase in residual compressive strength. At 800 °C,

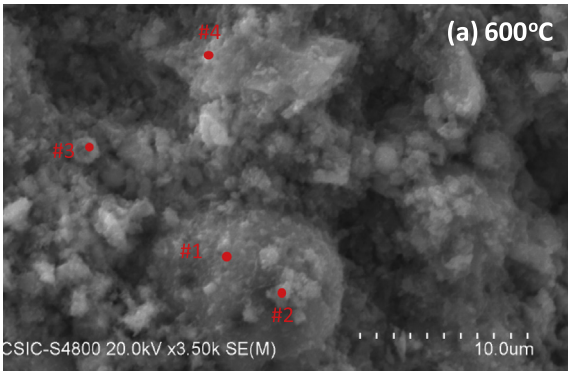

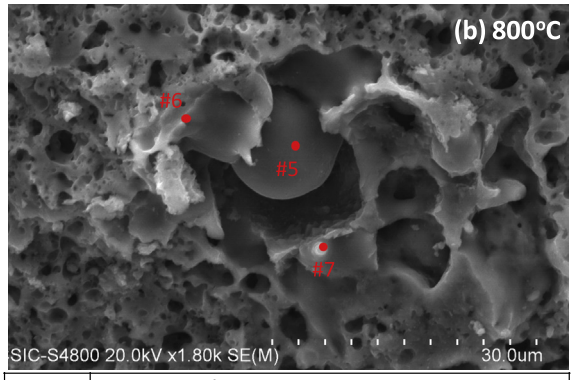

Point no.	O	Si	Al	Ca	Fe	S	K	Mg	Na
1	62,7	22,3	**8,79**	0,73	1,39	0,02	0,87	1,3	1,83
2	61,3	19,4	**10,1**	1,35	1,25	0,24	1,68	1,32	3,31
3	59,7	16,2	**9,06**	**7,09**	2,01	0,32	1,07	1,63	2,85
4	62,7	11,9	6,05	8,5	1,09	**5,91**	0,71	0,94	2,13
5	61,3	21,2	2,50	4,37	1,19	0,86	1,77	**5,45**	1,33
6	60,3	20,1	2,37	**10,5**	1,32		1,39	**3,98**	
7	59,4	17,5	4,37	**10,5**	1,77			**4,64**	1,84

Fig. 8. SEM–EDX data for FAN-4 pastes exposed to (a) 600 °C and (b) 800 °C. Both pastes were air cooled. EDX data is expressed as normalized atom%.

water is rapidly lost from cementitious gels and any ettringite present. Calcite will decarbonate to form free lime and release CO_2 gas. Any available sulphate can react with free lime to form anhydrite. All these processes were supported by the observations in XRD data for both MS and FAN-4 pastes.

The major difference between the two pastes was in the nature of new silicate based crystalline phases formed and the fact that in FAN-4, this was accompanied by shrinkage and increased strength, but in MS paste less shrinkage but major decreases compressive strength were observed. This section aims to discuss the possible reasons for these differences, which are undoubtedly linked to differences in elemental composition.

4.1. Reactions in the MS cement (high Ca/low Al)

The formation of significant quantities of dicalcium silicate type phases was noted in 800 °C treated MS pastes. Useful information on the phase transformations in MS cement can therefore be found by reference to work by authors attempting to synthesise low energy belite (Ca_2SiO_4) cements [35]. The aim of such works is to form reactive Ca_2SiO_4 compounds from suitable materials such as fly ash and $CaCO_3$ by firing at relatively low temperatures (800–1200 °C). In the paper by Pimraksa et al. [35], when the $CaO:SiO_2$ ratio of the system was fixed at 2, gehlenite ($Ca_2Al(AlSiO_7)$) formation was favoured over larnite (β-Ca_2SiO_4) between 1000–1200 °C. Furthermore, the reaction of quartz with free lime to form wollastonite ($CaSiO_3$) was observed by these authors at $CaO:SiO_2 = 2$ but

not when $CaO:SiO_2 = 3$. When the $CaO:SiO_2$ ratio was raised to 3, larnite formation became favourable over wollastonite. Our results differ from those of Pimraska et al., [35] since in the MS paste we can see in Fig. 7 that Larnite formation was favoured over Gehlenite even though the $CaO:SiO_2$ ratio was low (approx. 1.8 based on XRF data in Table 1). However, in broad agreement with these authors, when the $CaO:SiO_2$ ratio was lowered further (FAN-4 cement $CaO:SiO_2 = 0.28$), wollastonite and gehlenite formation were favoured over larnite.

Prior to heat treatment, the Ca-rich MS pastes consisted mainly of C–S–H gel, portlandite and calcite. Earlier studies with naturally occurring calcium silicate hydrate minerals such as tobermorite, hillebrandite and xonotlite have shown conversion to wollastonite, wollastonite plus portlandite or poorly crystalline larnite (α or β forms depending on temperature) when firing samples at up to 900 °C [36]. The evolution of C–S–H gel from PC hydration upon heating has been studied in detail by several authors. The gradual conversion of C–S–H gel to what was termed "a nesosilcate" from 200 to 750 °C has been monitored by ^{29}Si NMR [37]. These authors showed that after heating to 450 °C, existing Q^2 and Q^1 environments of the gel were decreased and new Q^1 and Q^0 environments formed. The new Q^0 environments correlated with XRD evidence for new compounds closely related to β-Ca_2SiO_4 phases. The growth in larnite content at the expense of C–S–H content during heating up to 620 °C, as measured by in situ neutron diffraction [38], generally supports the data of Alonso and Fernández [37] and agrees with the observations for our XRD data with MS pastes treated at 800 °C.

4.2. Reactions with the (low Ca/high Al) FAN-4 cement

Unlike the evolution of C–S–H gel to a poorly crystalline larnite polymorphs observed in MS pastes, the products in FAN-4 pastes were completely different. This is undoubtedly aided by the formation of a molten phase at 705 °C, within which solid state reactions can occur. The formation of a molten phase was considered as problematic by Skvara et al., [39] and in situ strength measurements of alkali activated fly ash pastes showed that strengths greatly increased upon cooling but were not representative of paste strengths while actually subjected to heat treatment [40]. Molten phase formation can cause plastic deformation in load bearing samples but can also help fill in existing cracks generated by thermal stress or chemical reactions that cause shrinkage effects. Whether molten phase formation is detrimental or beneficial will depend on the extent of the molten phase formed and its viscosity. The comparatively high Fe content in FAN-4 cement (see Table 1) and the possible formation of Fe-silicates has been said to lower sintering temperatures of fly ash based mixtures [41]. The significantly higher Na and K contents (again see Table 1) in FAN-4 pastes coupled with the presence of reacted fly ash glassy phases may also contribute to the low sintering temperature in a similar way as Na is well known to lower the melting point of silica glass.

A useful comparison is with materials known as alkali activated fly ash cements and metakaolin geopolymers. Their compositions are generally very low in Ca and relatively rich in Na. The cementitious gels in these systems are proposed to be 3-D crosslinked aluminosilicate networks of tetrahedrally linked groups with Na^+ ions acting as counter ions to the negative charge generated by tetrahedrally bonded Al atoms [42–44]. The gel has been previously labelled as N–A–S–H [45] and is also considered as a poorly ordered zeolite precursor due to the fact that prolonged curing at moderately elevated temperatures (60–200 °C) results in the transformation of the gel to various zeolites [46]. The Si:Al ratio has also been shown to be important in zeolite formation from these systems [47]. However, no zeolite phases were observed by XRD analysis of heat treated FAN-4 pastes. This suggests that the limited Ca content of the FAN-4 binder was sufficient to inhibit zeolite formation.

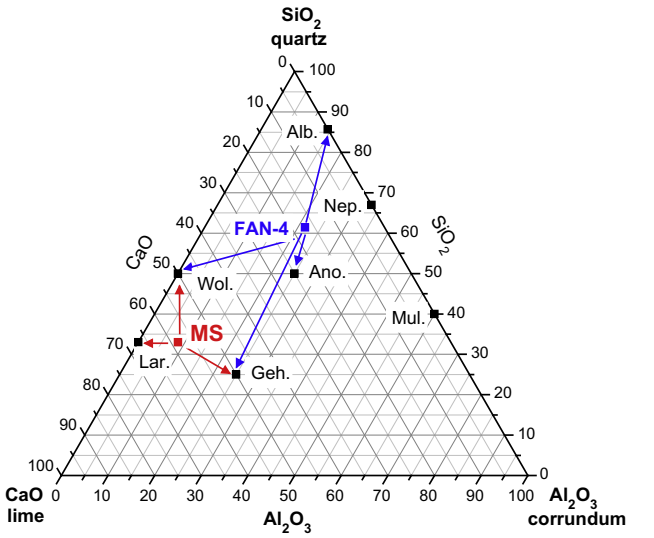

Fig. 9. Illustration of the location of MS and FAN-4 cement on ternary diagrams for (a)SiO_2–Al_2O_3–CaO and (b)SiO_2–MgO–CaO. Arrows indicate the shift to crystalline phases after firing at 800 °C as implied by XRD data. Phase labels correspond as follows: Alb. = albite ($NaAlSi_3O_8$); Aker. = akermanite ($Ca_2MgSi_2O_7$); Ano. = anorthite ($CaAl_2Si_2O_8$); Diop. = diopside ($CaMgSi_2O_6$); Geh. = gehlenite ($Ca_2Al(AlSiO_7)$); Lar. = larnite (Ca_2SiO_4); Mul. = mullite ($3{\cdot}Al_2O_3{\cdot}2SiO_2$); Nep. = nepheline ($AlNa(SiO_4)$; Wol. = wollastonite ($CaSiO_3$).

At higher temperatures relevant for comparison with this study, Bakharev [48] showed that class F fly ash activated by Na-activators formed nepheline ($NaAl(SiO_4)$) at 800 °C and albite ($NaAlSi_3O_8$) at 1000 °C, in good agreement with results published by Fernández-Jiménez et al. [49]. In other systems virtually free of Ca, the formation of Nepheline and other sodium aluminosilicates was shown to form upon heating beyond 850 °C [50,51]. Albite was also detected in FAN-4 pastes in this study but no nepheline. A number of different products in heated FAN-4 pastes such as gehlenite ($Ca_2Al(AlSiO_7)$), diopside ($CaMgSi_2O_6$) and wollastonite ($CaSiO_3$) were observed instead, undoubtedly due to the presence of higher quantities of Ca and limited quantities of Mg in FAN-4 pastes. The ternary diagram (SiO_2–Al_2O_3–CaO) relating the major elemental compositions of MS and FAN-4 cements and indicating the shifts to specific crystalline phases after heating at 800 °C, is given in Fig. 9.

The SiO_2–Al_2O_3–CaO ternary diagram illustrates a well balanced divergence of new crystalline phases in heated MS pastes and clearly shows that higher Ca content gehlenite was favoured over lower Ca anorthite. The same diagram also demonstrates that the low Ca and relatively high Al content in FAN-4 pastes effectively prohibit the formation of larnite. However, the Al/Na content of FAN-4 pastes was not high enough to favour Nepheline formation over Albite. In FAN-4 pastes, shifts to Si-enriched and Ca-enriched crystalline phases were noted but not to Al-enriched crystalline phases.

5. Conclusions

The temperature resistance of a novel low Ca content cement paste with approximately 20% clinker content (FAN-4) and a Type II/A-M Portland-composite cement paste with some 80–90% clinker content (MS) have been investigated. From the results presented, the following conclusions can be drawn:

- FAN-4 pastes exhibited a shift in colour from grey to red–orange between 600–800 °C, which was associated with the possible formation of Fe–silicates/hematite. This can be directly linked to Fe present in the majority fly ash component of the FAN-4 cement. No such drastic colour change was observed in the control MS cement. Slight yellowing at 1000 °C is likely to be due to sulfur formation from sulphides in any blast furnace slag present.
- Sintering occurred in FAN-4 pastes but not in MS pastes. The sintering event, and the fact that it occurred at a relatively low temperature may be linked to the much higher Fe content ($x3$) and higher total alkali content ($x2$) in FAN-4 pastes, having an analogous effect as in processes in the brick and glass industries respectively.
- Control MS pastes showed significantly greater weight losses upon heating at all temperatures, due to greater quantities of ettringite, gel H_2O, portlandite and calcite, which in turn is linked to the much greater ($x4$) clinker content in MS cement.
- Heating of the control MS pastes to 800 °C led to the conversion of cementious gel and CaO from dehydrated portlandite/decarbonated calcite to poorly crystalline calcium disilicate phases. The lower Ca and higher Al content in FAN-4 pastes favoured the formation of albite ($NaAl(SiO_4)$), anorthite ($CaAl_2Si_2O_8$), diopside ($CaMgSi_2O_6$), gehlenite ($Ca_2Al(AlSiO_7)$) and wollastonite ($CaSiO_3$).
- Such important differences in elemental composition and their influence on product behaviour should be considered when developing novel low CO_2 footprint binders in the future. The next logical step in this research would be to the assess performance of the FAN-4 binder in concretes with different aggregates and additives (super-plasticiser, air entraining agents etc.).

Acknowledgements

The authors acknowledge funding received which allowed this work to be carried out. This was via a research grant awarded to Ana Fernandez-Jimenez (BIA 2010:17530) from the Spanish Ministry of Science and Innovation and also the award of a JAE-Post doc scholarship to Shane Donatello co-funded by the aforementioned Ministry and the European Social Fund.

References

[1] Worrell E, Martin N, Price L. Potentials for energy efficiency improvement in the US cement industry. Energy 2000;25:1189–214.
[2] Habert G, Billard C, Rossi P, Chen C, Roussel N. Cement production technology improvement compared to factor 4 objectives. Cem Concr Res 2010;40:820–6.
[3] Gartner E. Industrially interesting approaches to "low-CO_2" cements. Cem Concr Res 2004;34:1489–98.
[4] Schneider M, Romer M, Tschudin M, Bolio H. Sustainable cement production – present and future. Cem Concr Res 2011;41:642–50.
[5] Lothenbach B, Scrivener K, Hooton RD. Supplementary cementitious materials. Cem Concr Res 2011;41(12):1244–56.
[6] ASTM C618–05. Standard specification for coal fly ash and raw or calcined natural pozzolan for use in concrete. ASTM International; 2005.
[7] EN 197–1. Cement – Part 1: composition, specifications and conformity criteria for common cements. European Standard, British version. ISBN 978 0 580 58045 1.
[8] Bentz DP, Ferraris CF. Rheology and setting of high volume fly ash mixtures. Cem Concr Comp 2010;32(4):265–70.
[9] Duran-Herrera A, Juarez CA, Valdez P, Bentz DP. Evaluation of sustainable high-volume fly ash concretes. Cem Concr Comp 2011;33(1):39–45.
[10] Kayali O, Sharfuddin Ahmed M. Assessment of high volume replacement fly ash concrete – concept of performance index. Constr Build Mat 2013;39:71–6.
[11] De Weerdt K, Kjellsen KO, Sellevold E, Justnes H. Synergy between fly ash and limestone powder in ternary cements. Cem Concr Comp 2011;33(1):30–8.
[12] Bentz DP, Sato T, de la Varga I, Jason Weiss W. Fine limestone additions to regulate setting in high volumen fly ash mixtures. Cem Concr Comp 2012;34(1):11–7.
[13] Palomo A, Fernández-Jiménez A, Kovalchuk G, Ordoñez LM, Naranjo MC. OPC-fly ash cementitious systems: study of gel binders produced during alkaline hydration. J Mat Sci 2007;42:2958–66.
[14] Donatello S, Fernández-Jiménez A, Palomo A. Very high volume fly ash cements. Early age hydration study using Na_2SO_4 as an activator. J Am Ceram Soc 2013;96(3):900–6.
[15] Donatello S, Fernández-Jiménez A, Palomo A. Durability of very high volume fly ash cement pastes and mortars in aggressive solutions. Cem Concr Comp 2013;38:12–20.
[16] Rostasy FS, Weib R, Wiedemann G. Changes of pore structure of cement mortars due to temperature. Cem Concr Res 1980;10(2):157–64.
[17] Skvara F, Sevcik V. Influence of high temperature on gypsum-free Portland cement materials. Cem Concr Res 1999;29:713–7.
[18] Khoury GA. Compressive strength of concrete at high temperatures: a reassessment. Mag Concrete Res 1992;44:291–309.
[19] Shoaib MM, Ahmed SA, Balaha MM. Effect of fire and cooling mode on the properties of slag mortars. Cem Concr Res 2001;31:1533–8.
[20] Yuzer N, Akoz F, Dokuzer Ozturk L. Comrpessive strength-color change relation in mortars at high temperature. Cem Concr Res 2004;34:1803–7.
[21] Aydin S, Baradan B. Effect of pumice and fly ash incorporation on high temperature resistance of cement based mortars. Cem Concr Res 2007;37:988–95.
[22] Mendes A, Sanjayan JG, Gates WP, Collins F. The influence of water absorption and porosity on the deterioration of cement paste and concrete exposed to elevated temperatures, as in a fire event. Cem Concr Comp 2012;34:1067–74.
[23] Xiao J, Falkner H. On residual strength of high-performance concrete with and without polypropylene fibres at elevated temperatures. Fire Safety J 2006;41:115–21.
[24] Debicki G, Haniche R, Delhomme F. An experimental method for assessing the spalling sensitivity of concrete mixture submitted to high temperature. Cem Concr Comp 2012;34:958–63.
[25] Wang HY. The effects of elevated temperature on cement paste containing GGBFS. Cem Concr Comp 2008;30:992–9.
[26] Anwar Hossain KM. High strength blended cement concrete incorporating volcanic ash: performance at high temperatures. Cem Concr Comp 2006;28:535–45.
[27] Phan LT, Carino NJ. Effects of test conditions and mixture proportions on behaviour of high-strength concrete exposed to high temperatures. ACI Mater J 2002;99(1):54–66.
[28] Behnood A, Ziari H. Effects of silica fume addition and water to cement ratio on the properties of high-strength concrete after exposure to high temperatures. Cem Concr Comp 2008;30(2):106–12.
[29] Donatello S, Tyrer M, Cheeseman CR. Comparison of test methods to assess pozzolanic activity. Cem Concr Comp 2010;32(2):121–7.
[30] Sarshar R, Khoury GA. Material and environmental factors influencing the compressive strength of unsealed cement paste and concrete at high temperatures. Mag Concrete Res 1993;45:51–61.
[31] Trindade MJ, Dias I, Coroado J, Rocha F. Mineralogical transformations of calcareous rich clays with firing: a comparative study between calcite and dolomite rich clays from Algarve. Portugal Appl Clay Sci 2009;42:345–55.
[32] Castellanos A, Mauricio O, Rios R, Alberto C, Ramos G, Angel M, Plaza P, Vinicio E. A comparative study of mineralogical transformations in fired clays from the Laboyos Valley. Upper Magdalena Basin (Columbia). Bol Geol 2012;34(1):43–55. <http://www.scielo.org.co/scielo.php?script=sci_arttext&pid=S0120-02832012000100003&lng=en&nrm=iso>. ISSN 0120-0283.
[33] Rickard WDA, van Riessen A. Thermal character of geopolymers synthesized from class F fly ash containing high concentrations of Iron and α-Quartz. Int J Appl Ceram Technol 2010;7(1):81–8.
[34] Garcia-Lodeiro I, Fernandez-Jimenez A, Palomo A, MacPhee DE. Effect on fresh C–S–H gels of the simultaneous addition of alkali and aluminium. Cem Concr Res 2010;40(1):27–32.
[35] Pimraksa K, Hanjitsuwan S, Chindaprasirt P. Synthesis of belite cement from lignite fly ash. Ceram Int 2009;35:2415–25.
[36] Shaw S, Henderson CMB, Komanschek BU. Dehydration/recrystallization mechanisms, energetic, and kinetics of hydrated calcium silicate minerals: an in situ TGA/DSC and synchrotron radiation SAXS/WAXS study. Chem Geo 2000;167:141–59.
[37] Alonso C, Fernández L. Dehydration and rehydration processes of cement paste exposed to high temperature environments. J Mater Sci 2004;39:3015–24.
[38] Castellote M, Alonso C, Andrade C, Turrillas X, Campo J. Composition and microstructural changes of cement pastes upon heating, as studied by neutron diffraction. Cem Concr Res 2004;34:1633–44.
[39] Skvara F, Jilek T, Kopecky L. Geopolymer materials based on fly ash. Ceram-Silik 2005;3:195–204.
[40] Fernandez-Jimenez A, Pastor JY, Martin A, Palomo A. High-temperature resistance in Alkali-activated cement. J Am Ceram Soc 2010;93(10):3411–7.
[41] Bijen JMJM. Manufacturing processes of artificial lightweight aggregates from fly ash. Int J Cem Comp Lightweight Concr 1986;8(3):191–9.
[42] Palomo A, Grutzeck MW, Blanco MT. Alkali-activated fly ashes. A cement for the future. Cem Concr Res 1999;29:1323–9.
[43] Fernández-Jiménez A, Palomo A, Criado M. Alkali activated fly ash binders. A comparative study between sodium and potassium activators. Mater Constru 2006;56(281):51–65.
[44] Duxson P, Fernandez-Jimenez A, Provis JL, Lukey GC, Palomo A, van Deventer JSJ. Geopolymer technology: the current state of the art. J Mater Sci 2007;42:2917–33.

[45] García-Lodeiro I, Fernández-Jiménez A, Palomo A, Macphee DE. Effect of calcium additions on N–A–S–H cementitious gels. J Am Ceram Soc 2010;93:1934–40.
[46] Geopolymers DavidovitsJ. Inorganic polymeric new materials. J Therm Anal 1991;37:1633–56.
[47] Kovalchuk G, Fernández-Jiménez A, Palomo A. Alkali-activated fly ash: effect of thermal curing conditions on mechanical and microstructural development – Part II. Fuel 2007;86:315–22.
[48] Bakharev T. Thermal behaviour of geopolymers prepared using class F fly ash and elevated temperature curing. Cem Concr Res 2006;36:1134–7.
[49] Fernández-Jiménez A, Palomo A, Pastor JY, Martín A. New cementitious materials based on alkali-activated fly ash: performance at high temperatures. J Am Ceram Soc 2008;91:3308–14.
[50] Krivenko PV, Kovalchuk GY. Directed synthesis of alkaline aluminosilicate minerals in a geocement matrix. J Mater Sci 2007;42:2944–52.
[51] Kuenzel C, Grover LM, Vandeperre L, Boccaccini AR, Cheeseman CR. Production of nepheline/quartz ceramics from geopolymer mortars. J Eur Ceram Soc 2013;33(2):251–8.